RSC Pharmaceutics

ROYAL SOCIETY OF CHEMISTRY

PAPER

View Article Online
View Journal | View Issue

Cite this: *RSC Pharm.*, 2025, **2**, 147

Systematic antimicrobial, biofilm, free radical inhibition and tyrosinase inhibition assessments of efficient green silver nanoparticles from the aqueous root extract of *Cyphostemma adenocaule* (*CA*)

Kamalakkannan Kaliappan,*[a] Pradeep Nagarajan,[a] Jayaprakash Jayabalan,[b] Hemalatha Pushparaj,[c] Selvaraja Elumalai,[d] Baranidharan Paramanathan,[b] Vijayabaskaran Manickam,[e] Huyn Tae Jang[f] and Ganesh Mani *[g]

A novel, fast and optimized etiquette for the production of silver nanoparticles using the root extract of *Cyphostemma adenocaule* (*CA*) is reported in our study. This plant is known to possess many natural terpenes, glycosides and sterols, which can reduce $AgNO_3$ solution. Typical physiochemical analyses like UV-spectroscopy, scanning electron microscopy (SEM), transmission electron microscopy (TEM), powder X-ray diffraction (XRD), and Fourier transformed infrared spectroscopy (FTIR) were used to characterize and confirm the synthesis of the produced nanoparticles. The XRD and TEM analyses validated that the obtained particles were spherical shaped with the average size of 18 nm. The CA–AgNPs depicted excellent anti-bacterial activity against the studied gram (+ve) and (–ve) microorganisms and showed a very good *S. aureus* biofilm in a dose-dependent response (a maximum inhibition of 88% at a 125 μg mL^{-1} dose). Further results proved its ability to neutralize ABTS free radicals (96.5% neutralization was noted at a 200 μg mL^{-1} dose with the IC_{50} value of 48.62 μg mL^{-1}) and mushroom tyrosinase enzyme (tyrosinase is the enzyme responsible for hyperpigmentation) inhibition from 34.25% ± 3.68% to 90.90% ± 3.45%, with the highest activity at 100 μg mL^{-1}. The above results indicate the potential of silver nanoparticles as antibacterial and antioxidant agents and tyrosinase inhibitors in the food, cosmetics and medicinal industries.

Received 8th June 2024,
Accepted 15th November 2024

DOI: 10.1039/d4pm00173g

rsc.li/RSCPharma

Introduction

The millennia-old practices of traditional medicine across the globe have consistently favored the use of metals and metal-based herbal formulations for the treatment of contemporary health issues. Systems such as Siddha and Ayurveda from India, Unani from the Middle East, Homeopathy from Germany, and Traditional Chinese Medicine (TCM) have long endorsed the therapeutic application of metallic and metal oxide-based natural compounds for alleviating various maladies. Indian healers have been documented employing a synergy of herbo-mineral concoctions, an approach substantiated by the ancient writings of sages like Agasthiar and Bohar, which dates back to over 3000 years.[1–10] Within the realms of Siddha and ayurvedic medicines, several herbo-mineral formulations, known as Parpam (mineral and metal oxides), Chenduram (mineral or metal sulfides), Chunnam (caustic oxide), Pathangam (sublimation product), and aristas and basmas, continue to be utilized for a myriad of health conditions. Notably, Parpam and Chenduram are prized for their efficacy and longevity, boasting shelf lives extending beyond 75 years.[8–18] Despite the general consensus in modern medicine regarding the toxicity of metals in their ionic forms, such toxicities are purportedly mitigated or outrightly eliminated *via* specific purification procedures delineated in Siddha and Ayurveda.[19,20]

Metals and non-metals, including gold, silver, iron, copper, zinc, mercury, and arsenic, serve as fundamental components in herbo-metallic formulations predominant in various traditional Indian medicines. The esteemed 'Rasa Sastra' texts by the revered Siddha Nagarjuna detail methodologies for crafting diverse herbo-metallic preparations. Primarily, these con-

[a]*Department of Pharmaceutical Biotechnology, Nandha College of Pharmacy, Erode 638052, India. E-mail: car2203@gmail.com; Tel: +91-97895-02934*
[b]*Department of Microbiology, St. Joseph College of Arts and Science, Cuddalore 607001, India*
[c]*Department of Chemistry, Anna University, Chennai 600025, India*
[d]*Granules Pharmaceutical Inc, Chantilly, VA 20151, USA*
[e]*Department of Pharmaceutical Chemistry, J.K.K. Nattraja College of Pharmacy, Komarapalayam, Erode 638 183, India*
[f]*Department of Chemical Engineering, Hanseo University, Hanseo-1 Ro 46, Haemi-myun 31662, South Korea*
[g]*Department of Pharmaceutical Chemistry, Mookambika College of Pharmaceutical Sciences and Research, Kalappara Road, Ambika Nagar, Mannathoor, Muvattupuzha, Kerala 686667, India. E-mail: chemgans@gmail.com*

coctions, referred to as Basmasin Ayurveda and Parpam in Siddha, are synthesized by amalgamating metals with specific plant extracts, followed by repeated calcinations known as 'shodhan' in Ayurveda and 'pudam' in Siddha.[18–23] These traditional methodologies claim to attenuate the toxicological aspects of the medicines while simultaneously enhancing their therapeutic potency, contingent upon adherence to prescribed dosages. Moreover, contemporary assertions suggest that the metallic constituents within these formulations exist as ultrafine nanoparticles, facilitating their integration into the bloodstream.[20–26] Furthermore, mercury and lead is used in some of these formulations, despite their recognized toxicity in conventional medical paradigms.

Highlighting the intersection between traditional and modern medical practices, platinum(II) complexes and their analogs, such as carboplatin and oxaliplatin, have gained recognition for their cancer-fighting capabilities.[27,28,34] Additionally, chemical complexes incorporating iron(II), gold, and copper have established themselves as effective chelating anticancer agents.[29–32] Over the past decade, the development of therapeutic agents based on ruthenium and gold has gained momentum, offering a promising alternative to cisplatin due to their reduced cytotoxicity and enhanced anticancer properties.[33,34] During the COVID-19 pandemic, supplements based on zinc, magnesium, and calcium have proven invaluable in combating viral infections and other health complications. These instances underscore the pivotal role of metals and metal-based complexes not only in traditional medical systems but also within the realm of contemporary allopathic medicine.

Recent advancements in the green synthesis of metal and metal oxide nanoparticles underscore the confluence of traditional wisdom and modern scientific practices. The green synthesis approach has facilitated the rapid fabrication of nanoparticles derived from the transition and precious metals such as gold, silver, platinum, palladium, iron, as well as alkaline earth metals, including magnesium, zinc, and trace elements like arsenic and selenium.[24,25,35–40] Among these, silver nanoparticles have garnered significant attention due to their broad spectrum of activities encompassing antimicrobial, anticancer, enzymatic inhibition, biofilm disruption, anti-inflammatory, wound healing properties, and photocatalytic efficiency. This widespread functionality is attributed to their quantum-confined nature alongside a substantial surface-to-volume ratio. Recent innovations have leveraged various plants for the green synthesis of silver, gold, and zinc oxide nanoparticles. The effectiveness of plant-based materials in nanoparticle synthesis is attributed to the abundance of reductive primary and secondary metabolites, such as carbohydrates, amino acids, proteins, alkaloids, polyphenols, and terpenes, among others. These metabolites not only facilitate the reduction of metal ions into nanoparticles but also furnish a protective coating that impedes aggregation and prolongs shelf life, thereby mitigating the cost associated with external capping agents commonly required in chemical synthesis routes. Thus, green synthesis emerges as an environmentally benign alternative to traditional chemical approaches. However, it is important to note that while plant-based methodologies offer several advantages, microbial synthesis, another green method, necessitates stringent sterile conditions, potentially elevating production costs. In supporting this, numerous research studies have been reported for the synthesis of silver and gold nanoparticles using various kinds of plants such *as Salvia officinalis*,[41] *Mentha asiatica*,[42] *Swertia paniculate*,[43] *Laminaria japonica*,[45] *Sida cordata*,[45] *Achyranthes japonica*,[46] *Paeonia japonica*,[47] *Hydnocarpus alpina*[48] and by using microbes[49–52] and their conjugation with antibiotics to achieve synergism in activity.[53] The reported procedure resulted in Ag or Au nanoparticles with sizes ranging from 10–90 nm and with potent antimicrobial activities against the studied microbes.

Cyphostemma adenocaule (*Steud. ex A. Rich.*) (*CA*) is a tropical and climbing shrub with yellow flowerings that belongs to the Vitaceae Family from the Cyphostemma genus; the plant is widespread in Senegal to Eritrea, south to Angola, DR Congo, Malawi and Mozambique including India and Pakistan. It has a large, fleshy perennial root stock.[54–56] It is mainly used in traditional medicines for folk remedies in Kenya, Nigeria and South Africa. Its leaves in the raw or in the form of decoction mixed honey are used to treat cough. Concentrated infusion of leaves can be used as a purgative and to treat swellings in the abdomen.[57–63] Tannins present in its root act as an astringent, and macerated root extract was also used as a deworming agent. Further, the root has been used to treat malaria and syphilis and to prevent abortion. Though the leaf and root extract of the CA has been pronounced for its various pharmacological and nutritional values, its efficacy in the synthesis of metal/metal oxide nanoparticles, particularly, Ag, has not yet been studied. Considering this as an advantage, our present research aims to appraise the potential of CA root extract as a reductant for silver nanoparticles (AgNPs) and characterizing the AgNPs thus produced by the below listed physiochemical techniques like Fourier transform infrared spectroscopy, UV-Vis spectroscopy (UV-Vis), powder X-ray diffraction (PXRD), field emission scanning electron microscopy (FE-SEM), high-resolution transmission electron microscopy (HR-TEM) and dynamic light scattering (DLS) and extend the research by evaluating the antimicrobial activity, biofilm inhibition, ABTS free radical scavenging, mushroom tyrosinase inhibition and photocatalytic roles in *in vitro* models. The method explained herein is innovative in terms of the novel utilization of the said CA plant extract for AgNPs synthesis, its optimization procedure, milder conditions and fast progress in the synthesis. Further, this is the first report on the efficacy of the CA root extract in silver nanoparticle production.

Experimental sections

Materials and methods

Plant collection. The dried plant root was acquired from the Century Plant Nursery in Karnataka and was authenticated by

Professor Dr J. Jayaprakash, Professor, St Joseph College of Arts and Science, Tamil Nadu (India). An herbarium specimen with voucher no. 1075 of the plant has been preserved in the department (Fig. 1).

Preparation of the CA leaf extract. Approximately 100 g of *CA fresh* leaves were harvested from a local nursery, meticulously sliced into minor pieces, thoroughly rinsed with water, and subsequently extracted using a combination of maceration and decoction methods at 60 °C. The resulting filtrate was then concentrated *via* a rotary vacuum evaporator before being freeze-dried at −80 °C and sealed in an airtight container. The resultant dark brown extractive dry powder was preserved in a refrigerator at 4 °C for future applications.[64] The derived final extract was subjected to preliminary phytochemical investigations using the standard procedure.[65–67]

Green synthesis of AgNPs using the CA leaf extract

A 1% CA solution was prepared initially using the lyophilized leaf extract, which served as the precursor for AgNP synthesis. The AgNPs, synthesized with the CA extract, were obtained through a method slightly modified from previously described protocols.[45–48] Into a 100 mL solution of 0.1 M $AgNO_3$ in a flask, 50 mL of the diluted extract was incrementally added under continuous magnetic stirring at 500 rpm. The transition of the $AgNO_3$ solution from colourless to light yellow, culminating in a dark brown hue, was observed upon the extract's integration. Following the exhaustive addition of the extract to the $AgNO_3$ solution, the resultant CA–AgNPs were isolated by centrifugation at 10 000 rpm for 10 minutes using a high-speed cold centrifuge. The isolated AgNPs were thoroughly washed with water to eliminate any residual $AgNO_3$ and unreacted soluble phytoconstituents. Subsequently, these AgNPs were dried in a hot air oven maintained at 50 °C for 2–3 hours. The dried AgNPs were then powdered using a mortar and stored in light-resistant containers for subsequent characterization purposes. This process was iterated to amass an adequate quantity of CA–AgNPs for comprehensive characterizations.

Fig. 1 Image of *Cyphostemma adenocaule* (*CA*).

Reaction condition optimization

Study on the effect of extract quantity on AgNP synthesis. To facilitate the optimal synthesis of CA–AgNPs, a defined volume of 2 ml of 0.1 M $AgNO_3$ solution was treated with varying volumes of the root extract solution (2, 4, 6, 8, 10, and 12 mL). With each increment of the extract, the solution's plasmon resonance absorbance was meticulously monitored, aiming to identify the maximal extract volume necessary to yield a substantial quantity of CA–AgNPs at ambient temperature.[47]

Study on the effect of temperature. To ascertain the optimum temperature necessary for synthesizing a high yield of CA–AgNPs, a predetermined volume of 0.1 M $AgNO_3$ solution combined with an optimized amount of the extract was incubated at various temperatures (25, 30, 40, 50, and 60 °C). Modifications in the surface plasmon resonance (SPR) absorbance at 419 nm were meticulously recorded. The formation of nanoparticles was analyzed by measuring the absorbance at the plasmon resonance wavelength peaks associated with the initial CA–AgNP formation and charting these values to ascertain the optimal temperature necessary for achieving high yields.

Study on the time required for the reaction. To ascertain the optimal duration necessary to generate a high yield of CA–AgNPs in the shortest possible time, experiments were conducted using a fixed volume of 0.1 M $AgNO_3$ solution. An optimized quantity of the extract was introduced at a controlled temperature, and the reaction was allowed to proceed at various intervals (15, 45, 60, 90, and 120 min), during which the SPR absorbance changes at 419 nm were meticulously recorded. Observations of nanoparticle formation were made by measuring the absorbance at the maximum plasmon resonance wavelength coinciding with the initial CA–AgNP formation. These measurements were then graphically represented to pinpoint the optimum duration for achieving a high nanoparticle yield.

CA–AgNP physiochemical characterization

Detection of plasmon resonance by UV-Visible spectroscopy. To confirm the synthesis of CA–AgNPs, the dried and powdered sample was dispersed in DI water and subjected to sonication. Subsequently, its absorbance was measured using a UV-visible spectrophotometer (Shimadzu–1240, Tokyo, Japan), scanning across the wavelength spectrum of 300–800 nm.

Fourier transform infrared spectroscopy (FTIR). The FTIR spectra for both the dried extract and the CA–AgNPs samples were acquired with a Nicolet 6700 FT-IR spectrometer at room

temperature (RT), employing the KBr pellet method. Specifically, 40 scanning cycles were utilized to capture the FTIR spectrum with a resolution of 4 cm^{-1}, spanning a spectral range from 4000 to 400 cm^{-1}.

Field emission scanning electron microscopy (FE-SEM). The surface morphology of the synthesized AgNPs was assessed utilizing FE-SEM (FE-SEM, JEOL Corp., JSM6700F). A properly sized specimen of CA–AgNPs was affixed to the aluminium stub of the scanning electron microscope using double-sided adhesive tape. Subsequently, the samples underwent a coating process with gold plasma using a sputter coater (Sputter Coater-108 Auto, Cressington).

High resolution transmission electron microscopy (HR-TEM). The morphology and dimensions of the synthesized CA–AgNPs were examined using a Hitachi-800 tunnelling electron microscope (Hitachi-800, Japan). The CA–AgNPs, dispersed in ethanol, were applied onto a copper grid of the TEM analyser, dried at ambient temperature, and subsequently positioned in the sample holder of the TEM instrument for analysis. The particle diameter of the CA–AgNPs was measured manually using the Image-J1 image processor and open-source software. About 200 individual particles were considered from three different TEM images, and the average diameter was computed statistically. Selected area electron diffraction (SAED) measurement was also conducted for the particles.

Powder XRD analysis. To elucidate the crystalline attributes of the synthesized CA–AgNPs, a comprehensive wide-angle powder X-ray diffraction (PXRD) analysis was conducted using a Rigaku Miniflex diffractometer equipped with Cu-Kα radiation (λ = 1.54 Å) across a 2θ span of 10°–80°, utilizing a step size of 0.1° and a dwell time of 1 s. The average particle size of the CA–AgNPs was determined employing Scherrer's equation (eqn (1))[47,48]

$$D = \frac{k\lambda}{\beta^{1/2}\cos\theta} \quad (1)$$

λ is the wavelength of X-rays (1.5418 Å), $\beta^{1/2}$ denotes the full width at half maximum (FWHM) of the XRD peak, k is the shape factor, and θ is the diffraction angle.

Dynamic light scattering and zeta potential analysis. Dynamic light scattering, also referred to as quasi-elastic light scattering, was employed to analyse the distribution of particle sizes and the characteristics of their movement within the medium. The light scattering and surface charge properties of the synthesized silver nanoparticles were measured using a Zetasizer from Malvern, version 6.20.

Antibacterial studies

The assessment of antibacterial activity was conducted by employing the agar well diffusion method. To ascertain the antibacterial efficacy of AgNPs, the following Gram-positive *Staphylococcus aureus* (MTCC 3160), *Yersinia enterocolitica* (MTCC 840), and Gram-negative *Shigella flexneri* (MTCC 1457), along with *Salmonella typhimurium* (MTCC 3224) pathogenic bacteria were selected and obtained from our microbiology department (Nadha College of Pharmacy, Erode, India), based on a previously established methodology with minor modifications.[45–47,65,68] Nutrient agar media was prepared, and 30–35 ml of this media was dispensed into sterile Petri plates. Following the solidification of the media, 100 µL of the working stock culture (1×10^6 cells per mL) was uniformly spread using a sterile cotton swab, and holes of 0.5 cm diameter were created using stainless steel cylinders. Various concentrations of serially diluted CA–AgNPs (50, 100, 150, and 200 µg mL^{-1}) were added to the wells in the Petri dishes. Thereafter, the plates were incubated at 37 °C for 24 hours in a BOD incubator.

Antibiofilm assay

The *in vitro* microtitre plate method was utilized to assess the extent of biofilm formation and its inhibition by CA–AgNP.[45,47,69]An overnight culture of the drug-resistant *S. aureus* and *E. coli* in LB broth and Brain Heart Infusion (BH) broth was used to access the biofilm inhibition of two selected strains in two different media. The cultures were subsequently diluted to achieve a final cell count of 5×10^{-5} CFU mL^{-1}. Following this, 10 µL of the culture was dispensed into the wells of a microtitre plate, and then 10 µL of CA–AgNPs at varying concentrations (0–250) µg mL^{-1} were added. The assembly was incubated at 37 °C for 24 h. Post incubation, the wells were meticulously rinsed with phosphate-buffered saline (PBS) to eliminate free-floating bacterial cells. The biofilm thus formed was fixed *via* the addition of 200 µL of 0.1% crystal violet in acetic acid for 10 minutes. Any excess stain was eliminated by washing with DI water and left to dry briefly. The dye bonded to the bacterial biofilm was extracted using 200 µL of 95% ethanol. The absorbance of the ethanolic crystal violet solution was then measured at 620 nm using the Agile ELISA reader, enabling the quantification of cells with biofilm-forming capabilities. Both negative and positive controls were incorporated into the assay for comparative analysis. The same procedure was repeated for the *E. coli* also in both LB and BH broths. The percentage biofilm inhibition was calculated using the following equation (eqn (2))

$$\%\ \text{biofilm inhibition by CA} - \text{AgNp}'\text{s} = 1 - \left(\frac{\text{Aborbance of cell treated with TS} - \text{AgNPS at 620 nm}}{\text{Absorbance of untreated control at 620 nm}}\right) \times 100 \quad (2)$$

ABTS scavenging assay

$ABTS^+$ radicals were generated through the reaction of potassium persulfate (2.5 mM) with ABTS (7 mM) at a 1 : 1 (v/v) ratio, and subsequently, the mixture was shielded from light and maintained at 25 °C for 10–15 hours before its application. The reagent solution underwent dilution with methyl alcohol until it reached an absorbance of 0.700 at 734 nm. Various concentrations of silver NPs (1 mL; ranging from 25 to 200 µg mL^{-1}) were amalgamated with the $ABTS^+$ solution (4 mL), and

the absorbance was recorded after a period of 30 min. These antioxidant assays were systematically executed in triplicate.[71]

The calculation of the percentage ABTS inhibition was implemented utilizing the ensuing formula (eqn (3)).

$$\text{Percentage ABTS inhibition}(\%) = \left[\frac{(\text{control abs}) - (\text{sample abs})}{(\text{control abs})} \times 100\right] \quad (3)$$

Mushroom tyrosinase assay

The mushroom tyrosinase (Sigma Chemical Co.) was employed for an *in vitro* bioassay following a reported procedure with certain modifications.[46] In short, phosphate buffer (20 mM, pH 6.8) 140 μl, mushroom tyrosinase (125 μg mL^{-1} in DI water) 20 μl, and green synthesized CA–AgNPs inhibitor solution 20 μl with concentrations ranging from 50 to 200 μg mL^{-1} were dispensed into the wells of a 96-well microplate. Similarly, water (the dispersion medium for CA–AgNPs) functioned as a negative control, while Kojic acid, a well-recognized tyrosinase inhibitor at 60 μg mL^{-1}, was employed as a positive control for the assay. Following pre-incubation for 10 minutes at room temperature, 20 μL of L-dopa (3,4-dihydroxyphenylalanine, 0.85 mM) was added, and the plate was subsequently incubated at 30 °C for 20 minutes. The absorbance of dopachrome was then measured at 491 nm using a microplate reader (Agile Microplate Reader, USA). Kojic acid served as the reference inhibitor, and phosphate buffer alone was utilized as the negative control. The inhibition efficacy of AgNPs was quantified as the percentage of concentration required to achieve a 50% inhibition rate (IC_{50}). This metric was derived from three separate experiments, each conducted in triplicate. The IC_{50} values were determined using data analysis and graphing tools, specifically Sigmaplot and Origin Pro, version 8.

Assessment of cytotoxicity using MTT assay

HT-29 cells were trypsinized, and the cell concentration was adjusted to 1.0×10^6 cells per mL in Roswell Park Memorial Institute (RPMI) medium, enriched with 10% heat-inactivated fetal bovine serum (FBS) and 1% penicillin/streptomycin. About 100 μL of this diluted cell suspension (1×10^4 cells per well) was dispensed into each well of a 96-well plate and incubated for 24 hours to promote partial monolayer formation. After incubation, the supernatant was carefully removed, and the monolayer was washed with a fresh medium. The cells in the selected wells were then treated with 100 μL of CA–AgNPs at various concentrations (32.5, 65, 130, and 260 μg mL^{-1}) in deionized water. The plates were incubated in a CO_2 incubator at 37 °C with 5% CO_2 and 95% relative humidity for an additional 24 hours. Following this period, the supernatants were discarded, and the cells received 20 μL of MTT solution (2 mg mL^{-1} in phosphate-buffered saline). The plates were incubated for another 4 hours under the same conditions. Afterward, any unreacted dye and media were removed, and the formazan crystals were dissolved in 100 μL of dimethyl sulfoxide. The absorbance of the formazan solution was measured at 570 nm using a microplate reader (Agile Reader, ACT Gene, USA). A negative control (untreated) and a positive control (5-fluorouracil at an IC50 concentration of 10 μg mL^{-1}) were also included for comparative analysis. The percentage of cell viability was calculated using the following formula, eqn (4):

$$\text{Viable cells}\ (\%) = \frac{\text{Abs of sample} - \text{Abs of blank}}{\text{Abs of control} - \text{Abs of blank}} \times 100 \quad (4)$$

Blank refers to the background, which means the solution without cells.

Statistical evaluation

Statistical analyses were performed utilizing the SigmaPlot-10.0 package. Student's *t*-test was utilized to decide significant contrasts between the output with p values ($p < 0.05$).

Results and discussion

Phytochemical screening

The results from phytochemical screening reveal the presence of phytoconstituents such as proteins, carbohydrates, phytosterols, terpenes, glycosides, among others. The findings correspond closely with those reported in prior studies by other researchers.[65–67] Primary metabolites, including carbohydrates, reducing sugars, flavonoids, and hydroxyl terpenes, are identified as potent agents for reducing $AgNO_3$ into AgNPs (Ag^0) in the synthesis process of AgNPs. Secondary metabolites like proteins, tannins, and glycosides, present in the extract, are purported to play a crucial role in the stabilization of Ag-nanoparticles, serving as a protective capping layer on the surface of the AgNPs thus formed. These metabolites are inclined to inhibit the agglomeration of nanoparticle clusters within the dispersed medium. Further, corroborative evidence from previous studies on the plant extract's ABTS activity also suggests that the extracts may be effective in reducing metal salts into their nanoparticle form.

UV-vis spectral characterization of CA–AgNPs

The transformation of the transparent $AgNO_3$ solution to a yellow, and finally, a dark brown colour (Fig. 2(a)) signals the successful synthesis of AgNPs through the introduction of the CA leaf extract solution. In contrast, the reference control comprising solely the $AgNO_3$ solution exhibited no change in colour over time, underscoring the necessity of both $AgNO_3$ and the leaf extract for the successful generation of CA–AgNPs. The surface plasmon resonance (SPR) spectra of the resultant CA–AgNPs colloidal solution, depicted in (Fig. 2(b)), demonstrate a surface plasmon resonance peak at 419 nm,[47] further corroborating the formation of AgNPs. The analysis indicates that the synthesized CA–AgNPs are approximately 20 nm in size, aligning with previous studies relating to size-dependent plasmon resonance.[71,72] The proposed mechanism for the formation of CA–AgNPs from aqueous $AgNO_3$ illustrated in Fig. 2(c) represents the reduction of $AgNO_3$ by myricetin isolated by Gebrehiwot *et al.* (2024).In the initial step, $AgNO_3$

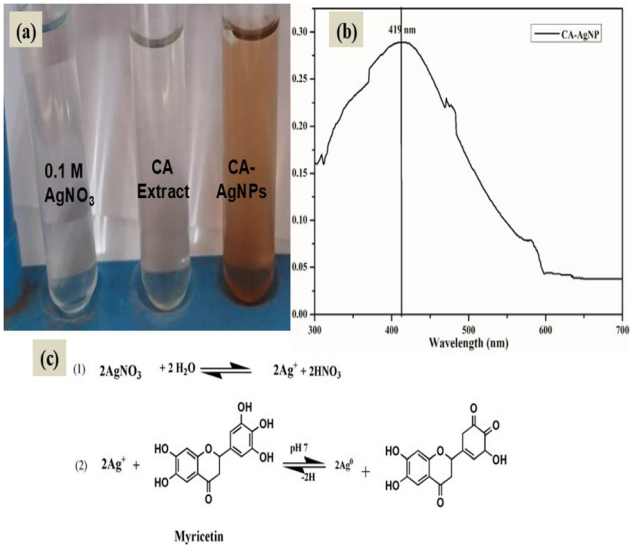

Fig. 2 (a). Synthesis of silver nanoparticles with CA leaf extract (b) SPR spectra of CA–AgNPs, (c) plausible mechanism of formation of CA–AgNPs.

dissociates into Ag^+ ions and nitric acid. Subsequently, Ag^+ ions undergo reduction to Ag^0, facilitated by the reducing metabolites present in the extract, such as myricetin, polyphenols, reducing sugars, and reductive metabolic enzymes (NAD and NADPH). These components donate electrons for the reduction process. This is followed by the nucleation and growth of nanoparticles, which are stabilized by the surface capping agents, including tannins and other polymeric substances.[61]

Optimization of reaction conditions

Effect of the quantity of CA leaf extract. The impact of the extract volume on the synthesis of CA–AgNPs was investigated by maintaining the concentration and volume (ml) of the $AgNO_3$ solution constant while varying the CA-extract volume (1% solution) between 2 to 10 mL in distinct test tubes. UV spectral scans post CA–AgNPs formation revealed a single overlay spectrum in Fig. 3, evidencing a characteristic plasmon resonance absorbance spectrum akin to preliminary findings. Notably, the color intensity of the $AgNO_3$ solution augmented with the increased extract volume up to a 5 mL extract to 2 mL of 0.1 M $AgNO_3$ solution ratio (Fig. 3). Subsequent addition of the extract (exceeding 5 mL) resulted in minimal or no significant changes in plasmon resonance absorbance, indicating that the maximum effective volume of 1% extract for the comprehensive conversion of Ag^+ ions to Ag^0 nanoparticles is 5 ml, deemed the optimal volume for complete reduction of Ag^+ ions in the solution. These findings demonstrate the enhanced efficacy of the CA extract at this optimized volume, which was subsequently employed for further optimization studies involving reaction time and temperature.[43,45]

Effect of temperature on AgNPs formation. Fig. 4 presents the UV-Vis spectra for the CA leaf extract plus $AgNO_3$ reaction

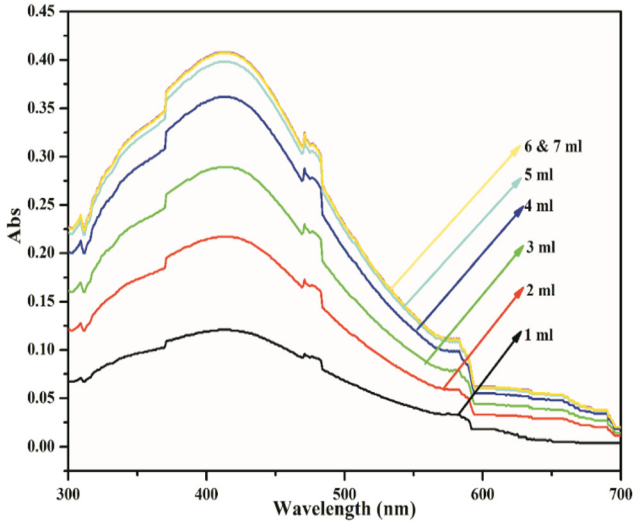

Fig. 3 Effect of extract quantity on AgNP synthesis (overlay).

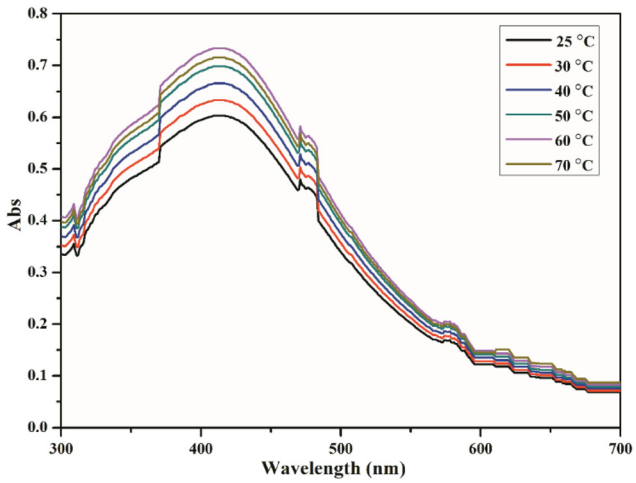

Fig. 4 Effect of temperature on CA–AgNPs synthesis.

mixture at various temperatures ranging from 25 to 60 °C. The absorbance peak, centred at approximately 419 nm, is attributed to the surface plasmon (SP) resonance of AgNPs, with its intensity varying according to the AgNPs concentration in the solution. Fig. 4 illustrates how the maximum absorbance of this peak correlates with temperature at a fixed heating duration. It is evident from Fig. 4 that the synthesis temperature significantly influences the intensity changes of the SP resonance band. At 25 °C, the CA–AgNPs formation process is markedly slow, with the resonance absorption intensity incrementally rising alongside the synthesis temperature, indicating that the increase in reaction temperature enhances the interactions between the bioactive compounds in the extract and the $AgNO_3$ molecules in the solution without reaching a point of saturation until the temperature hits 50 °C. At lower temperatures, a gradual rise in the intensity of the SP band *versus* temperature was observed, indicating a slower nanoparticle

growth rate as exemplified by the SPR bands at 25 °C and 30 °C in Fig. 4. Beyond this threshold, a temperature increment leads to accelerated collisions, thereby rapidly increasing the SPR intensity and causing a redshift indicative of larger particle sizes and aggregation and visually confirmed by precipitate formation at 60 and 70 °C. At 70 °C, the intensity of the SPR decreases due to the settling of aggregates, leaving a limited number of particles dispersed in the medium. These aggregates, or larger particles, exhibit diminished biological efficacy. Consequently, 50 °C was selected as the optimal temperature for synthesis. The lower operational temperature compared to that reported in other studies for the green synthesis of AgNPs using different plant extracts underscores the superior efficacy of the CA leaf extract in this synthesis process.

Effect of time on AgNPs formation. The influence of time on the formation of AgNPs was investigated over a duration of 1 hour, maintaining constant volumes of the extract and concentrations of $AgNO_3$ (0.1 mM $AgNO_3$ concentration and 5 ml of 1% v/v of the prepared extract) at an optimized temperature. According to the data shown in Fig. 5, a notable increase in the surface plasmon resonance (SPR) absorbance intensity was observed over time, peaking at 419 nm. The alteration in the SPR absorbance intensity at 419 nm, noticeable after 10 minutes of the reaction, signified the commencement of CA–AgNPs formation, which consistently intensified over time up to a certain point. Beyond this, further elongation in the reaction time managed to not only augment the intensity but also induce a red-shift, specifically from 420 to 425 nm. This shift denotes an increase in the nanoparticle size as a result of prolonged exposure time.[43] The absorbance continued to rise until the 40 minute mark, beyond which a plateau or minimal change in absorbance was noted, suggesting the depletion of reducible Ag^+ ions in the solution.[43,71] Thus, it was determined that the optimal conditions for the swift synthesis of CA–AgNPs are a 2 : 5 ml 0.1 M $AgNO_3$ to 1% extract ratio over a period of 40 minutes.

FTIR

To ascertain the major functional groups present in the CA extract and their potential roles in the formation and stabilization of AgNPs, FTIR spectral analyses were conducted. The FTIR spectrum of the CA extract powder is illustrated in Fig. 6. The FTIR spectrum of the CA extract unveiled multiple peaks, revealing its complex composition and concoction of various compounds. The vibrational band near 1610 cm^{-1} was attributed to the NH_2 group in the amino acids of proteins, while the bands at 1270 cm^{-1} corresponded to the stretching vibrations of the C–N amine bond. The band at 1160 cm^{-1} indicated the presence of (–CO–) carbonyl compounds. Moreover, a broad and overlapping band observed from 3000–3450 cm^{-1} was attributed to the –OH groups in phenolics and terpenes, as well as the NH group in amines. These findings suggest the presence of secondary metabolites akin to terpenoids, phytols, coumarins, *etc.*,[51,60–62]

The FTIR spectrum of CA–AgNPs, displayed in Fig. 7, demonstrates that nearly all significant vibrational bands identified in the FTIR spectrum of CA extract are also present here, albeit with diminished intensity relative to that of the CA leaf extract. The stretching vibration of the C=O bond of carboxylic acids or esters appeared near 1715 cm^{-1}, and the vibrational bands of nitro compounds and C–N amine bond were observed at 1634 cm^{-1} (NH_2 scissoring) and 1038 cm^{-1}. Analogous to the extract, a broad band from 3000–3450 cm^{-1} was assigned to the –OH groups in phenolics and terpenoids. This suggests that the secondary metabolites possessing these functionalities, such as polyphenolics, terpenoids, flavonoids, *etc.*, are considered responsible for the reduction of Ag^+ ions to Ag^0 nanoparticles and the subsequent stabilization of the formed nanoparticles by enveloping the particle surface.[43,45–48]

Electron microscopy results

Field emission scanning electron microscopy (FE-SEM). The FE-SEM images, as presented in Fig. 8, revealed the morpho-

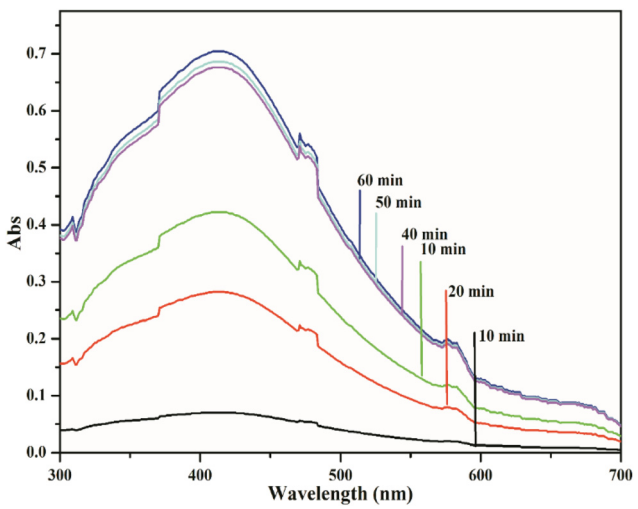

Fig. 5 Effect of time on CA–AgNPs synthesis.

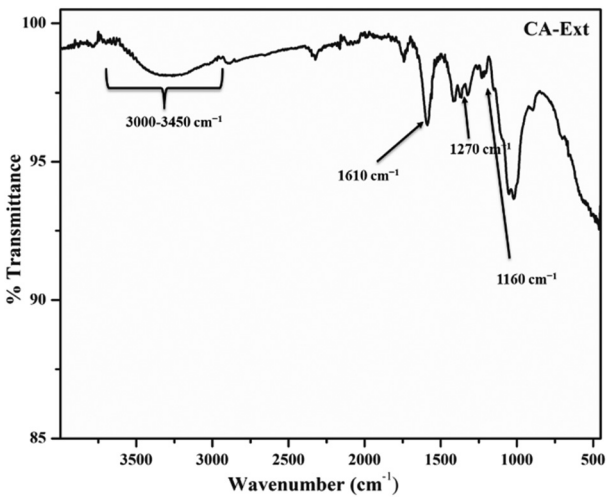

Fig. 6 FTIR spectra of CA leaf extract.

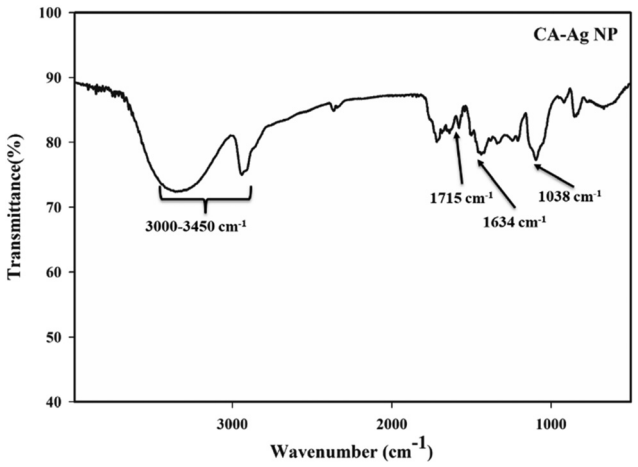

Fig. 7 FTIR spectra of CA–AgNPs.

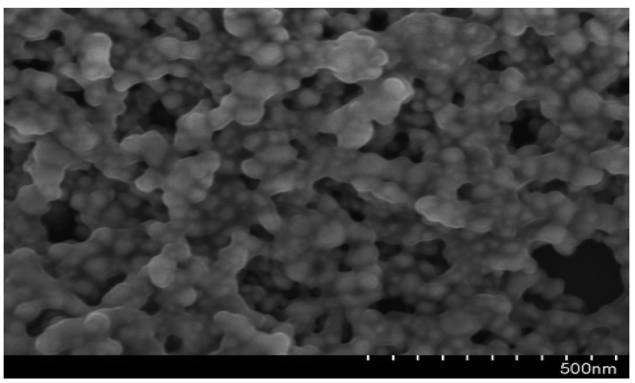

Fig. 8 FE-SEM images of CA–AgNPs at 500 nm magnification.

logical characteristics of the prepared CA–AgNPs. It was distinctly observed from the images that the manufactured nanoparticles predominantly exhibit a spherical morphology. Furthermore, the quantification of particle size, determined through the Image-J software analysis, yielded an average diameter of approximately 20 nm for the CA–AgNPs. This determination was based on the sizing of roughly 200 particles. The findings from these measurements are in alignment with the particle size previously reported, as corroborated by the UV-vis surface plasmon resonance data at 419 nm.[43,45–47]

High-resolution transmission electron microscopy (HR-TEM)

To further confirm the morphology of the CA–AgNPs synthesized by the optimized procedure, the high-resolution transmission electron microscopy (HR-TEM) technique was utilized, with the results presented in Fig. 9(a). A predominant presence of spherical/oval nanoparticles, with sizes ranging from 5 to 35 nm, was observed. The particle size distribution, as depicted in Fig. 9(insert), revealed that the majority of AgNPs had sizes within the 5 to 35 nm range, averaging 18 nm. The results indicate that the particles were dispersed well, maintaining separation from one another without any

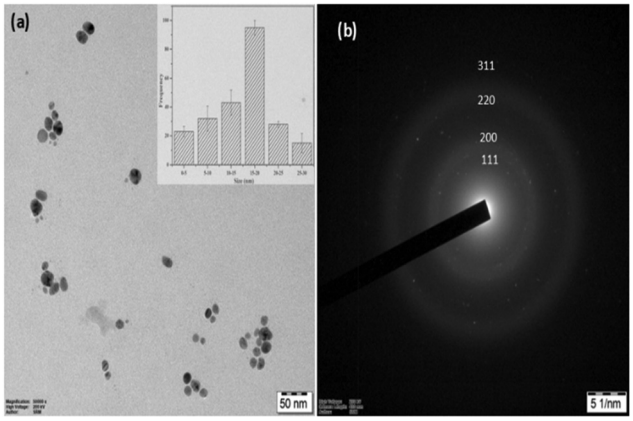

Fig. 9 (a) HR-TEM image of CA–AgNP. Inset: TEM-particle size distribution, (b) SAED pattern of the CA–AgNP.

clustering. This suggests a high level of stabilization afforded by the plant-derived capping agent. Further, the SAED pattern for the particle (Fig. 9(b)) shows concentric circular 2D patterns for lattice plane values of (111), (200), (220), and (311). This proves the face-centered cubic crystalline nature of the CA–AgNPs. This finding aligns with previous studies, which have demonstrated that plant biomolecules can serve as effective capping agents, significantly enhancing the re-dispersibility of green-synthesized AgNPs.[47,70]

XRD characterization. XRD traces were acquired to determine the crystalline nature of the green synthesized CA–AgNPs mediated by CA root extract. Fig. 10 illustrates the XRD pattern of the CA–AgNPs, where diffraction peaks observed at 2θ = 38.28°, 44.56°, 64.84°, and 78.18° have been indexed with the corresponding lattice plane values of (111), (200), (220), and (311). These results align with the standard XRD specifications for AgNPs established by the Joint Committee on Powder Diffraction Standards (JCPDS: 04-0783). The observed reflections denote the face-centered cubic (FCC) structure characteristic of AgNP. Utilizing Debye–Scherrer's equation and measuring the half-width of the most intense peak corresponding to the (111) lattice plane,[44–47] the average particle size of the

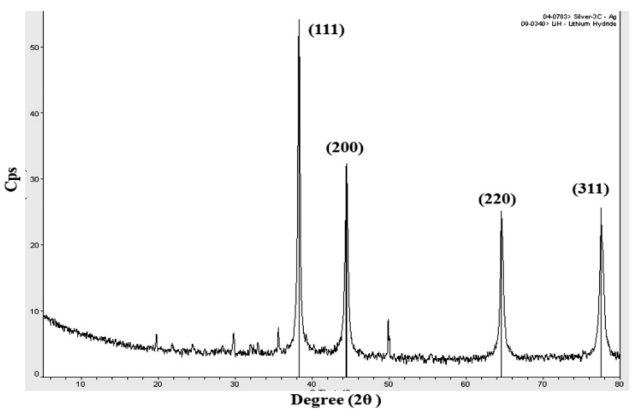

Fig. 10 XRD traces of CA–AgNPs.

AgNPs was calculated to be 20 nm. The presence of other pronounced peaks in the XRD pattern of CA–AgNPs indicates that the nanoparticles were efficaciously stabilized by the chemical constituents in the CA extract. These constituents may also play a role in reducing Ag^{+} ions in $AgNO_3$ solution to AgNP (Ag^0).[45–47] Meanwhile, co-existing peaks with lower intensity are attributed to organic impurities adhering to the sample.[43,46,47] The results for the XRD diffraction are further supported by the above TEM results.

DLS and zeta potential evaluation

The particle size distribution of the silver nanoparticle (CA–AgNP) mixture analysed using DLS is illustrated in Fig. 11(a). The results were greatly influenced by the larger particles, yielding a *z*-average size of 24 nm. Generally, DLS is known to be more responsive to larger particles, which implies that its measurements may not accurately reflect the characteristics of polydisperse samples. Additionally, the particle sizes obtained through UV-Vis spectroscopy and DLS were marginally larger than those measured by TEM and XRD. This discrepancy may arise from the fact that DLS and UV-Vis techniques assess hydrodynamic sizes rather than actual physical dimensions. Fig. 11(b) represents the surface charge of the nanoparticle as zeta potential. Zeta potential for the synthesized CA–AgNP was observed to be −18.9 mV, which proved the high stability of the particles formed in the study.

Antimicrobial activity

Fig. 12(a and b) presents the results of the antimicrobial properties exhibited by the CA–AgNPs. It was noted that the CA–AgNPs are more effective in inhibiting Gram-negative pathogenic bacteria than Gram-positive bacteria. The inhibition zones from the activity of CA–AgNPs against the Gram-negative *S. flexneri* and *S. typhimurium* bacteria were notably larger than those against the Gram-positive *S. aureus* and *Y. entercolitica*. Prior studies have demonstrated that AgNPs are potent against both multidrug-susceptible and multidrug-resistant strains of microbes. The precise mechanism underlying the antimicrobial properties of AgNPs against these pathogens remains elusive. Nevertheless, extensive research efforts have been dedicated to elucidating their mode of action, where three principal mechanisms have been thus far proposed: (i) damage to the cell wall and membrane, (ii) penetration and subsequent damage within the cell, and (iii) induction of oxidative stress.[71–76]

Antibiofilm activity

Fig. 13 illustrates the quantitative assessment of biofilm formation in response to various concentrations of CA–AgNPs, showing the percentage of biofilm inhibition for *S. aureus* and *E. coli* in the LB and BH broth. The results indicate that CA–AgNPs significantly inhibit biofilm formation for both bacterial species, even at sub-inhibitory concentrations ($p < 0.05$),

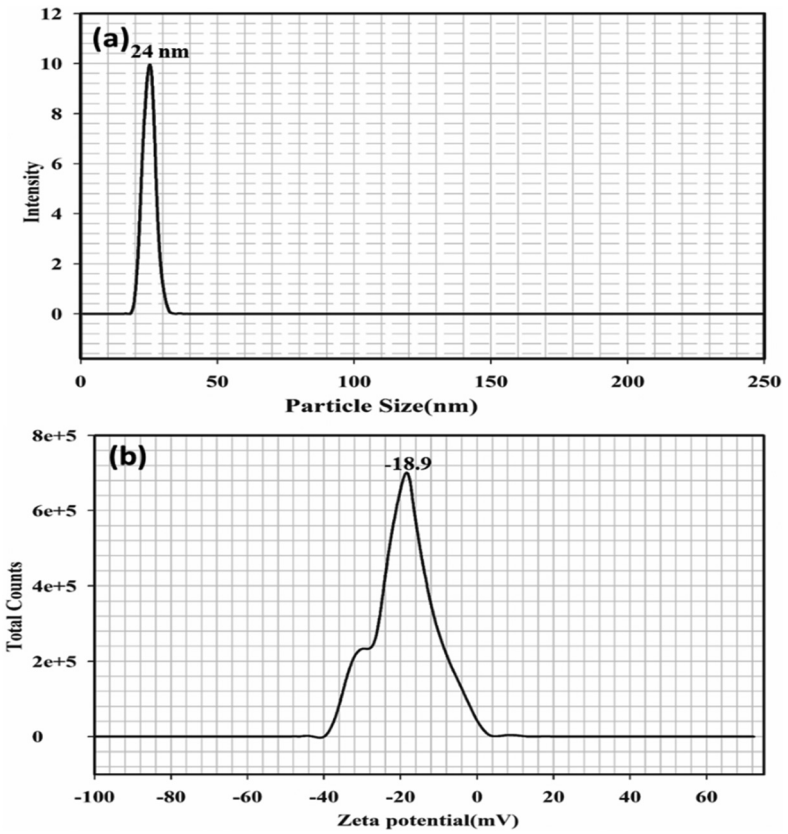

Fig. 11 (a) DLS particle size distribution (b) zeta potential of CA–AgNP.

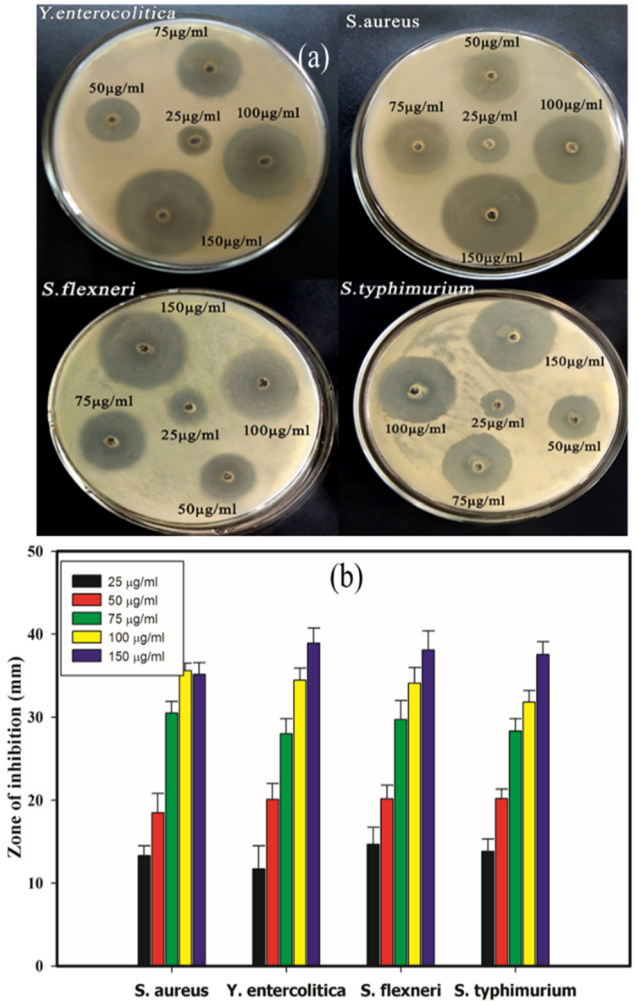

Fig. 12 Antimicrobial activity of CA–AgNPs (a) well diffusion sample image, (b) quantitative zone of inhibition.

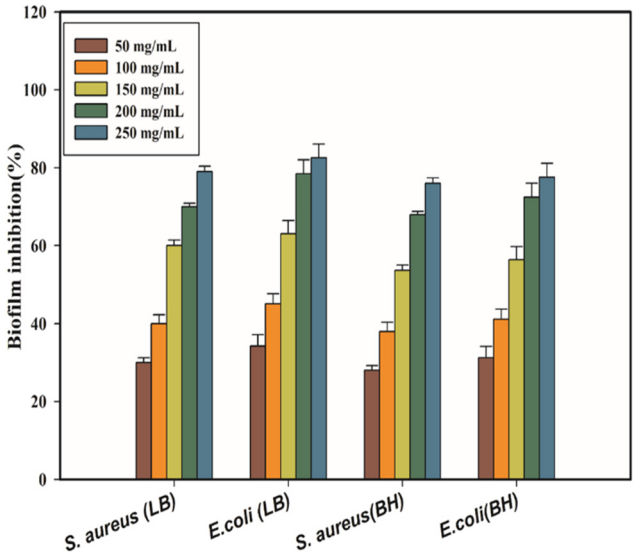

Fig. 13 Antibiofilm activity of CA–AgNPs.

in a concentration-dependent manner. Specifically, the inhibition of *S. aureus* biofilm reached a maximum of 79% in LB broth and 76% in BH broth at the highest concentration tested (250 µg mL^{-1}). Similarly, *E. coli* biofilm inhibition peaked at 82% in LB broth and 77% in BH broth at the same concentration. Notably, *E. coli* demonstrated a greater sensitivity to CA–AgNPs compared to *S. aureus*. Typically, biofilms offer microorganisms protection against environmental stresses such as changes in osmolarity, pH, and paucity of food and nutrients. Moreover, biofilms can impede the efficacy of antibiotics and shield the microorganisms from the host's immune responses.[43,69,79] As highlighted earlier, external stimuli on microbial cultures, particularly those forming biofilms, affect the production and release of *exo*-polysaccharides (EPSs). Metals and metal oxide nanoparticles, including Ag, Cu, and ZnO, have been shown to prevent EPS formation, thereby inhibiting biofilm development. This principle underpinned the inception of our AJ-NP anti-biofilm initiative. Given this, there is a pressing need for novel agents, beyond antibiotics, to counteract microbial biofilms. Biofilm inhibitors emerge as a promising solution to address the challenge of multi-drug-resistant bacteria. Numerous studies confirm the efficacy of metal and metal oxide nanoparticles in thwarting biofilm formation by target bacteria. Reports, including those by Goswami *et al.*, endorse the antimicrobial and anti-biofilm prowess of biogenically synthesized AgNPs, showing (5%–89%) biofilm inhibition against various pathogens.[77] Additionally, Gurunathan *et al.* conducted further studies on the anti-biofilm efficacy of synthesized AgNPs against pathogens like *P. aeruginosa*, *S. flexneri*, *S. aureus*, and *S. pneumoniae.* Their findings underscored significant anti-biofilm activity for AgNPs with particle sizes <100 nm, attributing inhibition of EPS synthesis to enhanced anti-biofilm effects. Despite biofilm EPS structures being rigid, they possess numerous pores and water channels, allowing small and nearly spherical nanoparticles to penetrate biofilms and effectively target and neutralize bacteria within. In summary, this study substantiates the efficacy of CA-mediated AgNPs as antibacterial and anti-biofilm agents. Previous research suggests that coupling AgNPs with antibiotics like chloramphenicol, kanamycin, ampicillin, and sulfanilamide can synergize their effects. Combining AgNPs with chloramphenicol resulted in up to a 50% inhibition of *E. coli*, *S. typhimurium*, and *S. aureus* growth, with kanamycin co-administration elevating inhibition rates to 95%.[49] These findings advocate for a synergistic approach, highlighting that AgNPs can alter cellular integrity and membrane potential, thereby enhancing antibiotic entry and microbial eradication. In light of the remarkable antibacterial properties of silver nanoparticles, they have been successfully employed in antimicrobial bandages, wound care formulations, antibacterial textiles, and as microbial and biofilm inhibitors in dental and urinary catheter applications.[43,49,77–79]

ABTS free radical scavenging assay

Diseases such as Parkinson's disease, various neural disorders, mild cognitive impairment, and the aging process are primar-

ily attributed to the action of one or more free radicals, including hydroxyl, superoxide, and peroxide radicals. These radicals can be neutralized by the regular consumption of dietary antioxidants found in natural foods.[80] Recent studies have extensively documented the antioxidant properties of green-synthesized metal and metal oxide nanoparticles. In this study, the antioxidant behaviour of CA-mediated AgNPs was explored, focusing on its effectiveness in scavenging ABTS radicals, and this activity was benchmarked against ascorbic acid (AA), a well-known natural antioxidant. The outcomes of this examination are depicted in Fig. 14(a). The data from ABTS scavenging assays demonstrate that the CA–AgNPs exhibit notable antioxidant activity. The radical scavenging efficacy of the CA–AgNPs escalated with concentrations ranging from 25 to 200 μg mL^{-1}, showing an inhibition percentage spanning from 25.45% ± 1.98% to 96.5% ± 2.4% (Fig. 14(a)). Maximum ABTS inhibition of about 96.5% ± 2.4% was attained with 200 μg mL^{-1} of CA–AgNP dose. The IC_{50} value, the concentration needed to neutralize 50% of ABTS radicals, was determined to be 48.62 μg mL^{-1}. Though the exact mechanism for ABTS scavenging AgNP has not been well established, it is believed that the antioxidant molecules bound to the surface of the nanoparticle are responsible for the activity. The myricetin or other ceanothane triterpenoid antioxidants in the CA extract are capable of scavenging the ABTS cation radical produced with the aid of the oxidant. The activity of the CA–AgNP is higher than that of the CA-extract due to the AgNP size and high surface-to-volume ratio. Hence, the AgNP thus formed can carry a larger quantity of antioxidant molecules than the crude extract. The plausible mechanism behind the activity is represented in (Fig. 14(b)).[81,82]

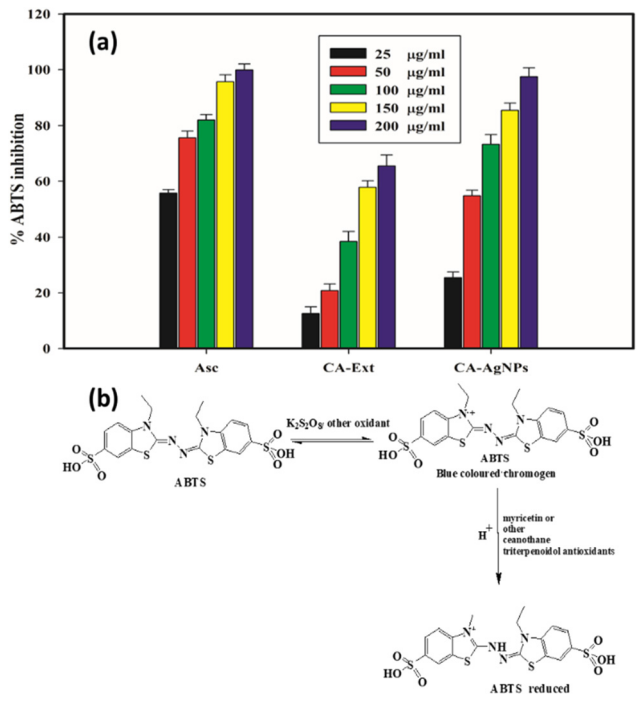

Fig. 14 (a) ABTS free radical scavenging activity, (b) plausible mechanism of ABTS radical inhibition.

Mushroom tyrosinase assay

The capability of CA–AgNPs to inhibit mushroom tyrosinase is depicted in Fig. 15. CA–AgNPs exhibited potent inhibitory effects on the mushroom tyrosinase enzyme, ranging from 34.25% ± 3.68% to 90.90% ± 3.45% at a concentration of 100 μg mL^{-1}. These inhibition levels were found to be on par with those of the standard Kojic acid at 60 μg mL^{-1}, which demonstrated an inhibition of 99.48% ± 2%. Moreover, the IC_{50}% value, indicating the amount of CA–AgNPs necessary to inhibit 50% of the mushroom tyrosinase activity, was determined to be 85.23 μg mL^{-1}. Tyrosinase, a copper-containing metalloenzyme, plays a pivotal role in melanin synthesis by converting tyrosine into di-hydroxyphenyl alanine (DOPA) and then to DOPA quinones, which polymerize to form melanin pigments. Inhibition of the tyrosinase enzyme, through the use of natural or synthetic antioxidants, is a strategy to prevent excessive melanin formation. A recent study by Armstrong *et al.* indicated that silver nanoparticles (AgNPs) disrupt copper homeostasis in cellular systems in a concentration-dependent manner.[83] This interference may represent a potential mechanism through which AgNPs regulate melanin production by inhibiting the activity of the enzyme tyrosinase (Fig. 16).[83,84]

Cytotoxicity activity by CA–AgNPs

The cytotoxic effects of CA–AgNPs on HT-29 cells are illustrated in Fig. 17. Treatment with 32.5 μg mL^{-1} of CA–AgNPs resulted in a significant decrease in cell proliferation, with a 44.8% reduction in cell viability compared to the untreated control (100% viability). The observed cytotoxicity was dose-dependent, peaking at the highest concentration of 260 μg mL^{-1}, which achieved a 76.8% inhibition of cell viability. Additionally, 5-fluorouracil (5-FU) at its IC_{50} concentration of 10 μg mL^{-1} produced a growth inhibition rate of 51.3%.

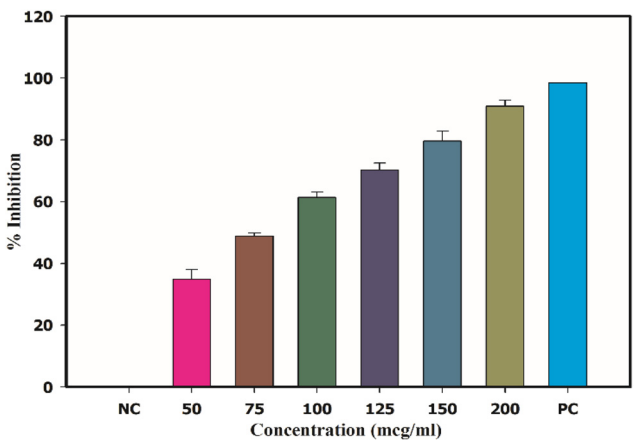

Fig. 15 Mushroom tyrosinase inhibition by CA–AgNPs.

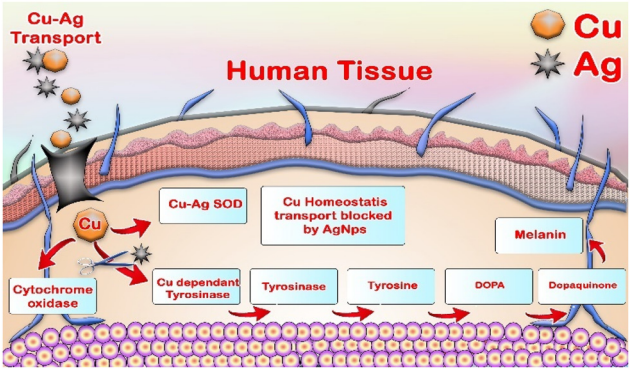

Fig. 16 Plausible mechanism of tyrosinase inhibition by AgNP.

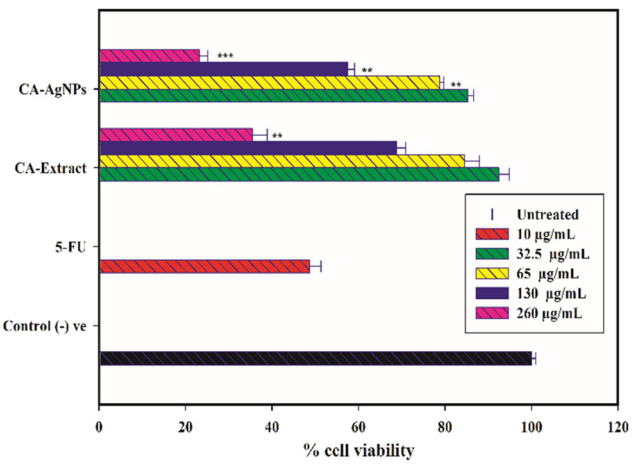

Fig. 17 Cytotoxic activity of CA–AgNPs (**$P < 0.01$, ***$P < 0.001$).

When compared to the 5-FU positive control, cells treated with CA–AgNPs at concentrations of 65 µg mL^{-1}, 130 µg mL^{-1}, and 260 µg mL^{-1} exhibited significantly different cytotoxic effects, with the corresponding *p*-values of $P < 0.01$, $P < 0.001$, and $P < 0.01$, respectively. These findings confirm that the synthesized nanoparticles possess potent cytotoxic activity against HT-29 cells. Notably, the cytotoxic effects of CA–AgNPs were more pronounced than those observed with CA extract alone. This discrepancy can be attributed to the presence of various metabolites in the crude extract, some of which may contribute to cytotoxicity while others may not, resulting in an overall diminished effect at higher concentrations.

In contrast, CA extract-coated AgNPs, due to their smaller size and larger surface area, showed enhanced efficacy. This aligns with previous studies suggesting that nanoparticles can penetrate cells more effectively, thereby apprehending their full potential.[85–87] Generally, the green-synthesized silver nanoparticles exhibit cytotoxicity against cancer cells through multiple mechanisms. AgNPs can (i) disrupt cellular signaling pathways, (ii) intercalate with DNA, leading to DNA damage and cell death, and increase the expression of caspase-3, promoting apoptosis. Moreover, AgNPs may disrupt the mitochondrial oxidative phosphorylation chain, which is often more active in cancer cells than normal cells. This disruption can result in the release of reactive oxygen species (ROS), triggering the release of cytochrome C into the cytosol, which in turn increases caspase protein expression and culminates in cell death.[85–87]

Conclusions

The results of the physiochemical analysis evidenced the successful transformation of silver nitrate into silver nanoparticles, with a size range of ~(5–35) nm and spherical morphology, with the aid of aqueous *Cyphostemma adenocaule* (*CA*) root extract through a novel green synthetic protocol. In addition, carbohydrates, phytosterols, terpenes, glycosides (as major components), proteins, polysaccharides, and phenolic compounds are expected to act as a reductant cum stabilizing agent in green synthesis. Similarly, the nanoparticles thus synthesized herein had the ability to inhibit the growth of microorganisms belonging to Gram (−ve) and Gram (+ve) pathogens and are efficient in biofilm inhibition against *S. aureus* and *E. coli* biofilms. Additionally, it showed excellent ABTS free radical scavenging activity and cytotoxic and mushroom tyrosinase inhibition comparable to that of the standards used. From the results, we conclude that the silver nanoparticles synthesized using CA have the potential as a broad antibacterial, antibiofilm, antioxidant and mushroom tyrosinase inhibition agent in various industries, mainly chemical, food, and medicine, as an additive/protectant.

Data availability

All the data that support the findings of this research are included in the main manuscript.

Author contributions

Conceptualization and work was designed by Professor Ganesh M and Professor. Kamalakkannan K. and.; data collected by, Pradeep N., formal analysis was carried by professor Jang H. T.; investigation; resources, data curation; writing original draft carried by Dr Jayaprakash J., Dr Hemalatha P., and Baranidharan P.; writing review and editing by Professor Ganesh M. Project supervision. Kamalakkannan K., Data interpretation by Selvaraja K. and Professor Vijayabaskaran M., project administration; Professor Kamalakkannan K. and Ganesh M. All authors have read and agreed to the published version of the manuscript.

Conflicts of interest

The authors declare no conflict of interest.

Acknowledgements

The authors gratefully acknowledge the Nandha college of Pharmacy management and Hanseo University, South Korea, for their technical and research support to conduct the research successfully.

References

1 M. Rama Devi, G. V. Dayanand Reddy, P. Narasimha Kumar, P. Sathiyarajeswaran and P. Elankani, Herbomineral formulations safety and efficacy employed in siddha system of medicine: A Review, *Int. Res. J. Pharm.*, 2019, **10**, 16–24, DOI: 10.7897/2230-8407.10014.

2 S. Barathi and A. Amuthan, *Siddhars and Siddha Medicine: the forgotten Indian saints and their medical knowledge*, University News, 2013, p. 41e53.

3 B. Prakash, Use of metals in Ayurvedic medicine, *Indian J. Hist. Sci.*, 1997, **32**, 1–27.

4 E. Ernst, Toxic heavy metals and undeclared drugs in Asian herbal medicines, *Trends Pharmacol. Sci.*, 2002, **23**, 136–139.

5 K. N. K. Muthaliar and K. S. Uttamarayan, *Siddha Pharmacopoeia*, Parinilayam, Chennai, 1987, p. 160.

6 S. S. Savrikar, Use of metallic/mineral medicinal preparations in the management of disease, in *Proc. Seminar on Metals in Medicine; Ayurvedic and Modern View*, 2004, pp. 16–18.

7 V. N. Meenadevi, P. N. Prasad and K. Kalirajan, Standardization of Siddha drug Sanguparpam using infrared spectrum, *Int. J. Pharm. Technol.*, 2010, **2**, 634–641.

8 Y. Chen, J. Zou, H. Sun, J. Qin and J. Yang, Metals in Traditional Chinese medicinal materials (TCMM): A systematic review, *Ecotoxicol. Environ. Saf.*, 2021, **207**, 111311, DOI: 10.1016/j.ecoenv.2020.111311.

9 Y. Tsongkha and S. Zhao, The use of metals in Tibeto-Mangolian medicine and traditional Chinese medicine: gold and Silver as examples, *Stud. Hist. Nat. Sci.*, 2020, **3**, 307–320.

10 W. Lei, X. Yingqiu, M. Sandugash, P. Weiling and L. Erwei, Metal ions as effectual tools for cancer with traditional Chinese medicine, *Acupunct. Herb. Med.*, 2023, **3**, 296–308, DOI: 10.1097/HM9.0000000000000083.

11 M.B. Galib, M. Mashru, C. Jagtap, B. J. Patgiri and P. K. Prajapati, Therapeutic potentials of metals in ancient India: Areview through *Charaka Samhita*, *J. Ayurveda Integr. Med.*, 2021, **2**, 55–63, DOI: 10.4103/0975-9476.82523.

12 Caraka, *Caraka Samhitaa*, Choukhambha Sanskrit Sansthaan, Sutra Sthaana, 1/69, Varanasi, India, 2000.

13 S. P. Pandey and M. S. Sudheesh, Comparison of the toxicological effect of lead –based herbo-mineral preparation and their corresponding metal nanoparticles on enzymatic activity and growth of Bakers yeast, *Int. J. Pharm. Sci. Res.*, 2019, **10**, 4451–4461.

14 V. C. Jiji, S. Vasanth, P. Shanmugapriya, R. Madhavan, S. Murugesan, V. Manjari and M. Murugesan, Antimicrobial activity of padigalinga chenduram against enteric pathogens, *PharmaTutor*, 2014, **2**, 98–101.

15 B. Ilango, S. D. Sharief, K. Vinoth Kumar, R. Rajkumar, D. Prathiba and E. Sukumar, Histopathological studies of the effect of Naga Parpam, a Zinc based drug of Siddha medicine, in Rats, *J. Cell Tissue Res.*, 2009, **9**, 1869–1873.

16 S. Elansekaran, V. Thanigavelan and M. Logamanian, Physico chemical characterization of Linga Chendhuram, *IOSR*, 2016, **15**, 9–15, DOI: 10.9790/0853-1504140915.

17 M. M. Al-Ansari, A. J. A. Ranjit Singh, F. S. Al-Khattaf and J. S. Michael, Nano-formulation of herbo-mineral alternative medicine from linga chenduram and evaluation of antiviral efficacy, *Saudi J. Biol. Sci.*, 2021, **28**, 1596–1606, DOI: 10.1016/j.sjbs.2020.12.00.

18 N. Kannan, S. Balaji and N. V. Anil Kumar, Structural and elemental characterization of traditional Indian Siddha formulation, Thalagak karuppu, *J. Ayurveda Integr. Med.*, 2017, **8**, 184–189, DOI: 10.1016/j.jaim.2016.11.005.

19 V. Sathya, M. Velpandian, M. Ramani and M. Pitchiahkumar, Primitive approach on review of Siddha herbs, herbo-mineral formulation exhibiting antiviral, *Int. J. Pharma Bio Sci.*, 2014, **5**, 138–147.

20 N. G. Patel, Ayurveda: the traditional medicine of India, in *Folk Medicine; The Art and the Science*, ed. R. P. Steiner, American Chemical Society, Washington, DC, 1986, pp. 41–65.

21 R. C. Kapoor, Some observations on the metal-based preparations in the Indian Systems of Medicines, *Indian J. Tradit. Knowl.*, 2010, **9**, 562–575.

22 N. Oyuntsetseg, M. A. Khasnatinov, P. Molor-Erdene, J. Oyunbileg, A. V. Liapunov, G. A. Danchinova, S. Oldokh, J. Baigalmaa and C. Chimedragcha, Evaluation of direct antiviral activity of the Deva-5 herb formulation and extracts of five Asian plants against influenza A virus H_3N_8, *BMC Complementary Altern. Med.*, 2014, **14**, 235, DOI: 10.1186/1472-6882-14-235.

23 S. Sheikh, A. Srivastava, R. Tripathi, S. Tripathi, V. P. Trivedi and R. C. Saxena, Toxicity of A Novel herbo-mineral preparation Las01 on human cancer cell lines and Its safety profile in humans and animals, *J. Evidence-Based Complementary Altern. Med.*, 2012, 948375, DOI: 10.1155/2012/948375.

24 A. A. Alfuraydi, S. Devanesan, M. Al-Ansari, M. S. Al Salhi and A. J. A. Ranjit singh, Eco-friendly green synthesis of silver nanoparticles from the sesame oil cake and its potential anticancer and antimicrobial activities, *J. Photochem. Photobiol., B*, 2019, **192**, 83–89, DOI: 10.1016/j.jphotobiol.2019.01.011.

25 K. Saravanakumar, R. Chelliah, D. MubarakAli, D. H. Oh, K. Kathiresan and M. H. Wang, Unveiling the potentials of biocompatible silver nanoparticles on human lung carcinoma A549 cells and Helicobacter pylori, *Sci. Rep.*, 2019, **9**, 5787, DOI: 10.1038/s41598-019-42112-1.

26 K. Unni, B. S. Karalam and A. V. Vijayasankar, Scientific basis for the preparation and characterization of iron based traditional drug Annabhedi sindooram: a materialistic approach, *Int. J. Res. Ayurveda Pharm.*, 2013, **4**, 149–152, DOI: 10.7897/2277-434304212.

27 A. Bindoli, M. Pia, G. Scutari, C. Gabbiani, A. Casini and L. Messori, Thioredoxin reductase: a target for gold compounds acting as potential anticancer drugs, *Coord. Chem. Rev.*, 2009, **253**, 1692–1707, DOI: 10.1016/j.ccr.2009.02.026.

28 T. C. Johnstone, K. Suntharalingam and S. J. Lippard, Third row transition metals for the treatment of cancer, *Philos. Trans. R. Soc., A*, 2015, **373**, 20140185, DOI: 10.1098/rsta.2014.0185.

29 U. Ndagi, N. Mhlongo and M. E. Soliman, Metal complexes in cancer therapy – an update from drug design perspective, *Drug Des., Dev. Ther.*, 2017, **11**, 599–616, DOI: 10.2147/DDDT.S119488.

30 K. Balamurugan and W. Schaffner, Copper homeostasis in eukaryotes: teetering on a tightrope, *Biochim. Biophys. Acta*, 2006, **1763**, 737–746, DOI: 10.1016/j.bbamcr.2006.05.001.

31 A. Gupte and R. J. Mumper, Elevated copper and oxidative stress in cancer cells as a target for cancer treatment, *Cancer Treat. Rev.*, 2009, **35**, 32–46, DOI: 10.1016/j.ctrv.2008.07.004.

32 S. R. Pattan, S. B. Pawar, S. S. Vetal, U. D. Gharate and S. B. Bhawar, The scope of metal complexes in drug design – a review, *Indian Drugs*, 2012, **49**, 5–12.

33 M. S. Salga, H. M. Ali, M. A. Abdulla and S. I. Abdelwahab, Acute oral toxicity evaluations of some zinc(II) complexes derived from 1-(2- Salicylaldiminoethyl) piperazine schiff bases in rats, *Int. J. Mol. Sci.*, 2012, **13**, 1393–1404, DOI: 10.3390/ijms13021393.

34 I. Kostova, Ruthenium complexes as anticancer agents, *Curr. Med. Chem.*, 2003, **13**, 1085–1107, DOI: 10.2174/092986706776360941.

35 A. A. A. Ljabali, Y. Akkam, M. S. Al Zoubi, K. M. Al-Batayneh, B. Al-Trad, O. Abo Alrob, A. M. Alkilany, M. Benamara and D. J. Evans, Synthesis of Gold nanoparticles using leaf extract of ziziphus zizyphus and their Antimicrobial Activity, *Nanomaterials*, 2018, **8**, 174, DOI: 10.3390/nano8030174.

36 K. K. Bharadwaj, B. Rabha, S. Pati, T. Sarkar, B. K. Choudhury, A. Barman, D. Bhattacharjya, A. Srivastava, D. Baishya, H. A. Edinur, Z. Abdul Kari and N. H. Mohd Noor, Green synthesis of Gold nanoparticles using plant extracts as beneficial prospect for cancer theranostics, *Molecules*, 2021, **26**, 6389, DOI: 10.3390/molecules26216389.

37 S. S. Salem, M. S. E. M. Badawy, A. A. Al-Askar, A. A. Arishi, F. M. Elkady and A. H. Hashem, Green biosynthesis of Selenium nanoparticles using orange peel waste: characterization, antibacterial and antibiofilm activities against multidrug-resistant bacteria, *Life*, 2022, **12**, 893, DOI: 10.3390/life12060893.

38 V. Cittrarasu, D. Kaliannan, K. Dharman, V. Maluventhen, M. Easwaran, W. C. Liu, B. Balasubramanian and M. Arumugam, Green synthesis of selenium nanoparticles mediated from *Ceropegia bulbosa* Roxb extract and its cytotoxicity, antimicrobial, mosquitocidal and photocatalytic activities, *Sci. Rep.*, 2021, **11**, 1032, DOI: 10.1038/s41598-020-80327-9.

39 S. E. Abdelazeem, F. Manal, H. Mohamed, M. A. E. M. Eman, M. T. Tamer and M. O. Ahmed, Green synthesis of platinum nanoparticles using atriplex halimus leaves for potential antimicrobial, antioxidant, and catalytic applications, *Arabian J. Chem.*, 2022, **15**, 103517, DOI: 10.1016/j.arabjc.2021.103517.

40 S. Vinodhini, B. S. M. Vithiya and T. A. A. Prasad, Green synthesis of palladium nanoparticles using aqueous plant extracts and its biomedical applications, *J. King Saud Univ., Sci.*, 2022, **34**, 102017, DOI: 10.1016/j.jksus.2022.102017.

41 M. Saravanan, S. K. Barik, D. Mubarakali, P. Prakash and A. Pugazhendhi, Synthesis of silver nanoparticles from Bacillus brevis (NCIM 2533) and their antibacterial activity against pathogenic bacteria, *Microb. Pathog.*, 2018, **116**, 221–226, DOI: 10.1016/j.micpath.2018.01.038.

42 D. Sarkar and G. Paul, Green synthesis of silver nanoparticles using mentha asiatica (Mint) extract and evaluation of their antimicrobial potential, *Int. J. Curr. Res. Biosci. Plant Biol.*, 2017, **4**, 77–82, DOI: 10.20546/ijcrbp.2017.401.009.

43 V. S. Ahluwalia, V. Elumalai, S. Kumar and R. S. Sangwan, Nano silver particle synthesis using *Swertia paniculata* herbal extract and its antimicrobial activity, *Microb. Pathog.*, 2018, **114**, 402–408, DOI: 10.1016/j.micpath.2017.11.052.

44 D.-Y. Kim, R. G. Saratale, S. Shinde, A. Syed, F. Ameen and G. Ghodake, Green synthesis of silver nanoparticles using *Laminaria japonica* extract: Characterization and seedling growth assessment, *J. Cleaner Prod.*, 2018, **172**, 2910–2918, DOI: 10.1016/j.jclepro.2017.11.123.

45 R. Brindhamani, M. Ganesh, P. Hemalatha, H. T. Jang and M. Vijayabaskaran, *Sida cordata* assisted bio-inspired Silver nanoparticles and its antimicrobial, free-radical scavenging, tyrosinase inhibition and photocatalytic activity (4 in 1 system), *Part. Sci. Technol.*, 2023, **41**, 626–639, DOI: 10.1080/02726351.2022.2129116.

46 O. G. Bhusnure, M. R. Bhokare, M. Ganesh, P. S. Giram, S. P. Sachin, J. Jayaprakash, K. Kamalakkannan, P. Hemalatha and H. T. Jang, Phytogenic synthesis of silver nanoparticles using *Achyranthes japonica* root and its *in vitro* antimicrobial, antioxidant, and mushroom tyrosinase inhibitions, *Part. Sci. Technol.*, 2024, **42**, 107–119.

47 M. Vijaybaskaran, M. Ganesh, M. Rajarajan, J. Jayaprakash and H. T. Jang, Rapid efficient green synthesis, optimization, characterization, *In vitro* Antibacterial, Biofilm Inhibition, and Free Radical Scavenging evaluation of Silver Nanoparticles using the medicinal plant *Paeonia*, *Inorg. Chem. Commun.*, 2024, **162**, 112199, DOI: 10.1016/j.inoche.2024.112199.

48 M. Ganesh, S. G. Lee, J. Jayaprakash, M. Mohankumar and H. T. Jang, *Hydnocarpus alpina Wt*extract mediated green

synthesis of ZnO nanoparticle and screening of its antimicrobial, free radical scavenging, and photocatalytic activity, *Biocatal. Agric. Biotechnol.*, 2019, **19**, 101129, DOI: **10.1016/j.bcab.2019.101129**.

49 J. Jayaprakash, M. Ganesh, K. Nandhini, P. Johnthomas, D. John Milton and H. T. Jang, Green biogenic synthesis of zinc oxide nanoparticles using *Pseudomonas putid*a, culture and its *In vitro* antibacterial and anti-biofilm activity, *Biocatal. Agric. Biotechnol.*, 2019, **21**, 101327, DOI: **10.1016/j.bcab.2019.101327**.

50 K. Saravanakumar, B. Sriram, A. Sathiyaseelan, A. V. A. Mariadoss, X. Hu, K. S. Han, V. Vishnupriya, D. Mubarakali and M. H. Wang, Synthesis, characterization, and cytotoxicity of starch-encapsulated biogenic silver nanoparticle and its improved anti-bacterial activity, *Int. J. Biol. Macromol.*, 2021, **182**, 1409–1418, DOI: **10.1016/j.ijbiomac.2021.05.036**.

51 M. Jeyaraj, G. Sathishkumar, G. Sivanandhan, D. MubarakAli, M. Rajesh, R. Arun, G. Kapildev, M. Manickavasagam, N. Thajuddin, K. Premkumar and A. Ganapathi, Biogenic silver nanoparticles for cancer treatment: an experimental report, *Colloids Surf., B*, 2013, **106**, 86–92, DOI: **10.1016/j.colsurfb.2013.01.027**.

52 J. Jayaprakash, P. Johnthomas, D. Johnmilton, C. Swaminathan, M. Sathish and M. Ganesh, Antibacterial and anti bio film activities of novel antibiotic conjugated silver nanoparticles, *Mater. Today: Proc.*, 2022, **49**(7), 2836–2841, DOI: **10.1016/j.matpr.2021.10.068**.

53 R. Shanmuganathan, D. Mubarakali, D. Prabakar, H. Muthukumar, N. Thajuddin, S. S. Kumar and A. Pugazhendhi, An enhancement of antimicrobial efficacy of biogenic and ceftriaxone-conjugated silver nanoparticles: green approach, *Environ. Sci. Pollut. Res. Int.*, 2018, **25**, 10362–10370, DOI: **10.1007/s11356-017-9367-9**.

54 **https://www.llifle.com/Encyclopedia/SUCCULENTS/Family/Vitaceae/28264/Cyphostemma_adenocaule** (accessed on 05-12-2023).

55 D. O. Ochwang'i, C. N. Kimwele, J. A. Oduma, P. K. Gathumbi, J. M. Mbaria and S. G. Kiama, Medicinal plants used in treatment and management of cancer in Kakamega County, Kenya, *J. Ethnopharmacol.*, 2014, **51**(3), 1040–1055, DOI: **10.1016/j.jep.2013.11.051**.

56 O. M. Bello, S. M. Jagaba, O. E. Bello, A. B. Ogbesejana, O. A. Dada, C. O. Adetunji and S. M. Abubakar, Phytochemistry, pharmacology and perceived health uses of non-cultivated vegetable *Cyphostemma adenocaule* (Steud. ex A. Rich.) Desc. ex-Wild and R. B. Drumm: A review, *Sci. Afr.*, 2019, **2**, e00053, DOI: **10.1016/j.sciaf.2019.e00053**.

57 D. Z. Matata, F. Machumi, O. D. Ngassapa, M. J. Moshi, F. M. S. Mafumik, K. Oosthuizen, B. Swanepoel, L. Venables, T. C. Koekemoer, P. E. Kazyoba and M. de Vente, Evaluation of Root Extract of *Cyphostemma Adenocaule* (Vitaceae) for Antioxidant Activity, Brine Shrimp Toxicity, and Antiproliferative Activity against Hela Cervical Cancer Cells, *Int. J. Med. Plants Nat. Prod.*, 2021, **7**, 19–27, DOI: **10.20431/2454-7999.0701003**.

58 A. H. Yakubu, M. M. Mohammed, A. B. Bababe and H. Braimah, Phytochemical screening, antioxidant and antibacterial activities of the root exrtract of *Cyphostemma adenocaule* (Steud.ex A. Rich.) Wild & R.B. Drumm, *Biol. Med. Nat. Prod. Chem.*, 2021, **10**(2), 105–110, DOI: **10.14421/biomedich.2021.102.105-110**.

59 G. Fikadu and G. Mulugeta, Phytochemical Investigation on the root of *Cyphostemma Adenocaule* (Steud. Ex A. Rich), *Alger. J. Nat. Prod.*, 2022, **10**, 904–917.

60 D. Abebe, G. Periasamy, A. Karim and H. Bitew, Evaluation of the Effect of Hydroethanolic Root Extract and Solvent Fractions of *Cyphostemma adenocaul*e, (Steud. ex A. Rich) descoings ex wild & drummond on cell-mediated immune response and blood cell count in mice, *Evidence-Based Complementary Altern. Med.*, 2021, 183890, DOI: **10.1155/2021/1838903**.

61 H. Gebrehiwot, A. Dekebo, K. Shenkute, U. Ensermu and M. Endale, Chemical composition, antibacterial and antioxidant activities of essential oils from *cyphostemma adenocaule* and *ziziphus Spinachristi*, *Bull. Chem. Soc. Ethiop.*, 2024, **38**, 167–186, DOI: **10.4314/bcse.v38i1.13**.

62 J. R. Chouna, F. Nardella, B. N. Lenta, C. V. Sénécheau, P. N.-E. Alango and N. Sewald, Ceanothane-type triterpenoids from *Cyphostemma adenocaule*, *Arch. Pharmacal Res.*, 2016, DOI: **10.1007/s12272-016-0801-1**.

63 T. Degfie, J. O. Ombito, T. B. Demissie, R. Eswaramoorthy, A. Dekebo and M. Endale, Antibacterial and antioxidant activities, in silico molecular docking, ADMET and DFT analysis of compounds from roots of C. cyphopetalum, *Adv. Appl. Bioinf. Chem.*, 2022, **15**, 79–97, DOI: **10.2147/AABC.S377336**.

64 M. Ganesh and M. Mohankumar, Extraction and identification of bioactive components in *Sida cordata* (Burm.f.) using gas chromatography–mass spectrometry, *J. Food Sci. Technol.*, 2017, **54**, 3082–3091, DOI: **10.1007/s13197-017-2744-z**.

65 A. R. Gulnaz and G. Savitha, Evaluation of antimicrobial activity of leaf and stem extracts of sidda medicinal Plant *Sida Cordata*, *Int. J. Med. Pharm. Sci.*, 2013, **3**, 39, DOI: **10.14260/jemds/570**.

66 J. B. Harborne, *Phytochemical methods: a guide to modern techniques of plant analysis*, Chapman and Hall, London, 1984, p. 84.

67 G. E. Trease and W. C. Evans, *Pharmacognosy*, Bailliere Tindall, London, 11th edn, 1989, p. 45.

68 M. Davoodbasha, S. C. Kim, S. Y. Lee and J. W. Kim, The facile synthesis of chitosan-based silver nano-biocomposites via a solution plasma process and their potential antimicrobial efficacy, *Arch. Biochem. Biophys.*, 2016, **605**, 49–58, DOI: **10.1016/j.abb.2016.01.013**.

69 M. H. Siddique, B. Aslam, M. Imran, A. Ashraf, H. Nadeem, S. Hayat, M. Khurshid, M. Afzal, I. R. Malik, M. Shahzad, U. Qureshi, Z. U. H. Khan and S. Muzammil, Effect of Silver nanoparticles on Biofilm formation and EPS pro-

duction of multidrug-resistant *K. pneumoniae*, *BioMed. Res. Int.*, 2020, 6398165, DOI: 10.1155/2020/6398165.

70 H. F. Hetta, I. M. S. A. Kadmy, S. S. Khazaal, S. Abbas, A. Suhail, M. A. E. Mokhtar, N. H. A. Ellah, E. A. Ahmed, R. B. Abdellatief, E. A. El Masry, G. E. S. Batiha, A. A. Elkady, N. A. Mohamed and A. M. Algammal, Antibiofilm and antivirulence potential of silver nanoparticles against multidrug-resistant Acinetobacter baumannii, *Sci. Rep.*, 2021, **11**, 10751, DOI: 10.1038/s41598-021-90208-4.

71 F. Khuda, M. Jamil, A. A. Khalil, R. Ullah, N. Ullah, F. Naureen, M. Abbas, M. S. Khan, S. Ali, H. M. U. Farooqi and M.-J. Ahn, Assessment of antioxidant and cytotoxic potential of silver nanoparticles synthesized from root extract of *Reynoutria japonica* Houtt, *Arabian J. Chem.*, 2022, **15**, 104327, DOI: 10.1016/j.arabjc.2022.104327.

72 J. Mock, M. Barbic, D. Smith, D. Schultz and S. Schultz, Shape effects in plasmon resonance of individual colloidal silver nanoparticles, *J. Chem. Phys.*, 2002, **116**, 6755, DOI: 10.1063/1.1462610.

73 N. H. Ibrahim, A. S. Awaad, R. A. Alnafisah, S. I. Alqasoumi, R. M. El-Meligy and A. Z. Mahmoud, *In vitro* activity of Desmostachya bipinnata (L.) stapf successive extracts against Helicobacter pylori clinical isolates, *Saudi Pharm. J.*, 2018, **26**, 535–540, DOI: 10.1016/j.jsps.2018.02.002.

74 T. C. Dakal, A. Kumar, R. S. Majumdar and V. Yadav, Mechanistic basis of antimicrobial actions of Silver nanoparticles, *Front. Microbiol.*, 2016, **7**, 1831, DOI: 10.3389/fmicb.2016.01831.

75 N. Durán, M. Durán, M. B. de Jesus, A. B. Seabra, W. J. Fávaro and G. Nakazato, Silver nanoparticles: a new view on mechanistic aspects on antimicrobial activity, *Nanomedicine*, 2016, **12**, 789–799, DOI: 10.1016/j.nano.2015.11.016.

76 Y. N. Slavin, J. Asnis, U. O. Häfeli and H. Bach, Metal nanoparticles: understanding the mechanisms behind antibacterial activity, *J. Nanobiotechnol.*, 2017, **15**, 65, DOI: 10.1186/s12951-017-0308-z.

77 S. R. Goswami, T. Sahareen, M. Singh and S. Kumar, Role of biogenic silver nanoparticles in disruption of cell–cell adhesion in Staphylococcus aureus and Escherichia coli biofilm, *J. Ind. Eng. Chem.*, 2014, **26**, 73–80, DOI: 10.1016/j.jiec.2014.11.017.

78 V. T. Noronha, A. J. Paula, G. Durán, A. Galembeck, K. Cogo-Müller, M. Franz-Montan and N. Durán, Silver nanoparticles in dentistry, *Dent. Mater.*, 2017, **33**, 1110–1126.

79 P. S. Stewart and J. W. Costerton, Antibiotic resistance of bacteria in biofilms, *Lancet*, 2001, **358**, 135–138.

80 S. Gurunathan, J. W. Han, D.-N. Kwon and J.-H. Kim, Enhanced antibacterial and anti-biofilm activities of silver nanoparticles against Gram-negative and Gram-positive bacteria, *Nanoscale Res. Lett.*, 2014, **9**, 373.

81 H. Gebrehiwot, Y. Melaku, M. Aliye, U. Ensermu, A. Dekebo, M. Endale, D. Rentsch and M. Hunsen, Antibacterial and antioxidant efficacies of secondary metabolites from the roots of *cyphostemma adenocaule*: A Combined *In Vitro* and *In Silico* Study, *J. Trop. Med.*, 2024, 1679695, DOI: 10.1155/2024/1679695.

82 A. Cano, A. B. Maestre, J. Hernández-Ruiz and M. B. Arnao, ABTS/TAC methodology: Main Milestones and recent applications, *Processes*, 2023, **11**(1), 185, DOI: 10.3390/pr11010185.

83 N. Armstrong, M. Ramamoorthy and D. Lyon, Mechanism of Silver Nanoparticles action on insect pigmentation reveals intervention of copper homeostasis, *PLoS One*, 2013, **8**, e53186.

84 M. Govindappa, H. Farheen, C. P. Chandrappa, R. V. Channabasava, V. Rai and B. Raghavendra, Mycosynthesis of silver nanoparticles using extract of endophytic fungi, Penicillium species of Glycosmis mauritiana, and its antioxidant, antimicrobial, anti-inflammatory and tyrosinase inhibitory activity, *Adv. Nat. Sci.: Nanosci. Nanotechnol.*, 2016, **7**, 035014.

85 Z. Jia, H. Sun and Q. Gu, Preparation of Ag nanoparticles with triethanolamine as reducing agent and their antibacterial property, *Colloids Surf., A*, 2013, **419**, 174–179, DOI: 10.1016/j.colsurfa.2012.12.003.

86 S. P. Dubey, M. Lahtinen and M. Sillanpää, Tansy fruit mediated greener synthesis of silver and gold nanoparticles, *Process Biochem.*, 2010, **45**, 1065–1071, DOI: 10.1016/j.procbio.2010.03.024.

87 S. H. M. Ghandehari and P. Ardalan, Anti-oxidant and cytotoxic properties of green synthesized silver nanoparticles from *Rubia tinctoru*, *Sci. J. Kurdistan Univ. Med. Sci.*, 2017, **26**, 57–67, DOI: 10.1049/iet-nbt.2018.5190.